Tectonophysics 581 (2012) 182–192

Contents lists available at SciVerse ScienceDirect

Tectonophysics

journal homepage: www.elsevier.com/locate/tecto

Intraplate earthquakes, regional stress and fault mechanics in the Central and Eastern U.S. and Southeastern Canada

Owen Hurd *, Mark D. Zoback

Department of Geophysics, Stanford University, 397 Panama Mall, Stanford, CA 94305-2215, USA

ARTICLE INFO

Article history:
Received 18 February 2011
Received in revised form 20 February 2012
Accepted 1 April 2012
Available online 13 April 2012

Keywords:
Intraplate seismicity
Crustal stress
Central and eastern United States
Focal mechanisms
Fault mechanics

ABSTRACT

Utilizing 75 high quality individual earthquake focal plane mechanisms and 10 formal stress inversions we investigate the consistency of regional stress orientations in the central and eastern United States and southeastern Canada, the variation of relative stress magnitudes across the region and the compatibility of slip on optimally-oriented nodal planes with frictional faulting theory. To map faulting styles and relative stress magnitudes across the region of study, we utilize the high quality focal plane mechanisms to calculate the AΦ parameter (following Angelier, 1979; Simpson, 1997) that ranges from 0 (uniform horizontal extension with $S_V >> S_{Hmax} = S_{hmin}$) to 1.5 (strike–slip faulting with $S_{Hmax} > S_V > S_{hmin}$) to 3 (uniform horizontal compression with $S_{Hmax} = S_{hmin} > S_V$). We find that horizontal stresses become increasingly more compressive with respect to the vertical stress from the south-central United States (characterized predominantly by strike–slip focal mechanisms) toward the northeastern U.S. and southeastern Canada (predominantly thrust mechanisms). In a manner similar to the study by M.L. Zoback (1992a), which used a much smaller data set, we utilize the Mohr–Coulomb criterion to calculate the difference in orientation between the theoretically-optimal orientation of a fault plane (for various coefficients of friction, μ) and the focal mechanism nodal planes assuming that pore pressure in the brittle crust is hydrostatic. For the 75 focal plane mechanisms utilized in our study, the preferred (better fitting) nodal planes deviate on average only 7° in strike and dip from the theoretically-optimal planes for $\mu = 0.6$. As such minor differences could represent small variations in the stress field (or uncertainties in the focal plane mechanisms), we conclude that nearly all earthquakes in the study region slip in a manner compatible with shear failure on pre-existing faults in the local stress field.

1. Introduction

Significant amounts of seismicity occur in intraplate regions throughout the world, often on tectonic structures such as pre-existing fault zones, sometimes associated with failed rifts, and ancient suture zones (e.g. Sykes, 1978). Intraplate seismicity in North America is frequently correlated with pre-existing faults which are optimally-oriented for reactivation in the current stress field (e.g., Zoback, 1992a; Zoback and Zoback, 1981). The stress field in the central and eastern United States (CEUS) and southeastern Canada is remarkably consistent on the lateral scale of 100 s of kilometers and is generally characterized by a horizontal, compressive, NE–SW trending maximum horizontal stress (e.g. Sbar and Sykes, 1973; Zoback and Zoback, 1980, 1991) thought to derive from buoyancy-driven forces such as ridge push (see Zoback and Zoback, 2007 for review) or from geoid perturbations and mantle thermal anomalies (Davies, 1999).

Second order stress fields, some of which may deviate from the large-scale regional field described above, are also observed across the CEUS. These stresses are generally driven by more localized buoyancy forces related to processes such as sediment loading and deglaciation or the presence of lateral lithospheric heterogeneities (e.g., Zoback and Mooney, 2003). The stresses generated by these processes may also contribute to the nucleation of intraplate seismicity in the CEUS and southeastern Canada. Since earthquakes are a direct result of stresses acting within the crust, analyzing seismicity in intraplate regions may yield valuable information regarding the current state of stress and physical conditions of the upper crust (pore pressure, fault friction) that is often unavailable from other sources. This information is essential to addressing potential seismic hazards in intraplate regions.

Earthquake focal plane mechanisms are often used to estimate the orientation of the three principal stresses (vertical stress (S_v), maximum horizontal stress (S_{Hmax}) and minimum horizontal (S_{hmin})) in the crust. The P-axis of the focal mechanism, which is defined as the

* Corresponding author. Tel.: +1 650 725 5831; fax: +1 650 725 7344.
E-mail addresses: ohurd@stanford.edu (O. Hurd), zoback@stanford.edu (M.D. Zoback).

0040-1951/$ – see front matter © 2012 Elsevier B.V. All rights reserved.
doi:10.1016/j.tecto.2012.04.002

bisector of the dilatational quadrants, is generally taken to represent the approximate orientation of S_{Hmax}, although it could significantly deviate from the true S_{Hmax} orientation in the absence of friction (McKenzie, 1969). In contrast to S_{Hmax} orientations estimated from individual focal mechanisms, a formal stress inversion of multiple earthquake focal mechanisms directly estimates the orientation of the three principal stresses and provides a more accurate S_{Hmax} orientation than the P-axis of an individual focal mechanism (Angelier, 1979; Gephart and Forsyth, 1984; Michael, 1984). The inversion procedure assumes a uniform stress field over the crustal volume containing all focal mechanisms used for the inversion and that shear slip occurs in the direction of maximum resolved shear stress (Bott, 1959).

In general, earthquake focal plane mechanisms are obtained from body-wave first-motions and polarizations (e.g. Khattri, 1973), body-wave amplitude ratios (e.g. Kisslinger et al., 1981), waveform modeling (e.g. Nábělek, 1984) or a combination of these methods. While the quality of an individual focal mechanism depends on the recording array geometry, seismogram signal-to-noise ratio and the accuracy of the earth velocity model, certain constraints generally yield higher quality and more reliable solutions. For example, because waveform modeling uses body-wave amplitude information and searches over a broader coverage of the focal sphere for a solution, it is often more powerful for constraining fault orientations than a focal mechanism created solely from P-wave polarities (e.g. Lay and Wallace, 1995). Solutions constrained by only P-wave polarities, for instance, may have several distinctly different nodal plane pairs (and slip configurations) that fit the data equally well and are highly dependent on recording array geometry. Consequently, we only consider high quality individual focal mechanisms constrained by waveform modeling in this study.

We compile well-constrained focal mechanisms and formal stress inversions from the CEUS and southeastern Canada over the past ~20 years. We utilize these data to investigate the consistency of regional stress orientations, to map faulting styles and relative stress magnitudes across the region and to investigate the likelihood of shear failure on the more well-oriented nodal planes in the local stress field in the context of frictional faulting theory, in a manner analogous to M.L. Zoback (1992a) who worked with a much smaller data set.

2. Data collection

All individual focal mechanisms and focal mechanism inversions are compiled from publications and earthquake catalogs over the past ~20 years. Since the individual focal mechanisms will directly be used to calculate relative stress magnitudes and examine slip compatibility in our analysis, it is crucial that the mechanisms be well constrained. To ensure such quality, we only select mechanisms constrained by waveform modeling. Again, waveform modeling techniques provide a better constraint on fault orientations because they use a broader coverage of the focal sphere along with relative body-wave amplitudes to constrain solutions.

The study area includes the CEUS, with the western boundary corresponding roughly to the 105°W line of longitude, and southeastern Canada. A total of 52 individual focal mechanisms and 10 stress inversions (from Mazzotti and Townend, 2010) are compiled (Appendices A and B, respectively). Of the 52 new focal mechanisms, 24 indicate thrust faulting, 25 are strike–slip and 3 represent normal faulting regimes. All focal mechanisms have magnitudes greater than $M_w = 3.1$ with the maximum magnitude being $M_w = 5.2$. The Canadian earthquakes range in depth from 2 to 25 km with an average depth of 14.1 km compared to a depth range of 2 to 18 km with an average of 8.0 km for the CEUS earthquakes. We also include 23 of the focal mechanisms analyzed by Zoback (1992a) within this study area (Appendix C). In instances where a precise latitude and longitude location are not available for a data point, a location is estimated using the original data source.

3. Defining stress orientations and relative stress magnitudes

3.1. Stress orientations

The first objective in our analysis is to investigate the consistency of the maximum horizontal principal stress orientation throughout the study area as inferred from the P-axes of newly compiled individual focal mechanisms and the formal stress inversions. Fig. 1 illustrates the new data points overlain on the 2008 World Stress Map (WSM) database (Heidbach et al., 2008), which is essentially identical to the database used by Zoback (1992a,b). In general, the S_{Hmax} orientations inferred from the new focal mechanisms (shown by blue bars on the black and white mechanisms) as well as the stress inversions (dark green circles with dark green bars) are consistent with the overall NE–SW S_{Hmax} orientation seen over much of the CEUS and southeastern Canada. Moreover, the new data points are locally consistent with pre-existing data which often show slight variations from the regional stress orientation.

This said, in contrast to the broadly homogeneous S_{Hmax} orientation, several focal mechanisms and stress inversions appear to indicate locally variable S_{Hmax} orientations. For example, the stress inversion in central Virginia yields a S_{Hmax} orientation of 90°, which is a roughly 45° clockwise rotation from stress indicators just to the west (Fig. 1). Similarly, the six new individual focal mechanisms in the Wabash Valley seismic zone in southern Illinois have an average P-axis orientation of 77°, which is relatively consistent with the regional S_{Hmax} direction but differs from the local E–W S_{Hmax} orientation indicated by nearby breakout stress indicators in western Kentucky and the focal mechanism inversion in the New Madrid seismic zone in NE Arkansas. Four of the five new data points in the Charlevoix seismic zone and both new focal mechanisms (and the stress inversion) in the St. Lawrence seismic zone also display a significant clockwise S_{Hmax} rotation from the regional trend as inferred from nearby borehole breakout measurements.

3.2. Relative stress magnitudes

The second objective is to estimate the relative magnitudes of the three principal stresses at hypocenteral depths. First, we estimate the local S_{Hmax} orientation near each earthquake from independent stress measurements in the WSM database. This is inferred by averaging the S_{Hmax} orientation from the three nearest data points in the WSM, regardless of type. If the standard deviation of the average is greater than 25°, the average of the two nearest ‘A’ quality stress measurements is used. For all 52 earthquakes, the two nearest ‘A’ quality stress measurements are usually from either borehole breakouts or hydraulic fractures. Next, to constrain the orientations of the remaining principal stresses S_{hmin} and S_V, we assume that the three principal stresses are perpendicular to one other and oriented horizontally and vertically (Zoback and Zoback, 1980). In Fig. 2 of Mazzotti and Townend (2010), it is clear that one principal stress is near vertical in each of the ten areas where focal mechanism inversions were carried out.

With the stress orientations constrained, the relative magnitudes of the three principal stresses are then calculated. Prior to calculation, the guidelines from Zoback (1992b) were used to classify each focal mechanism as thrust, strike–slip or normal. For S_V, we assume a regional lithostatic gradient of 25 MPa/km, which corresponds to an overburden density of 2500 kg/m^3. Although rock densities increase with depth, and a higher gradient (27–28 MPa/km) may be more appropriate for the earthquakes of greater depth, we use the 25 MPa/km gradient since the majority of earthquakes examined in this study fall within the upper crust. More importantly, since only relative

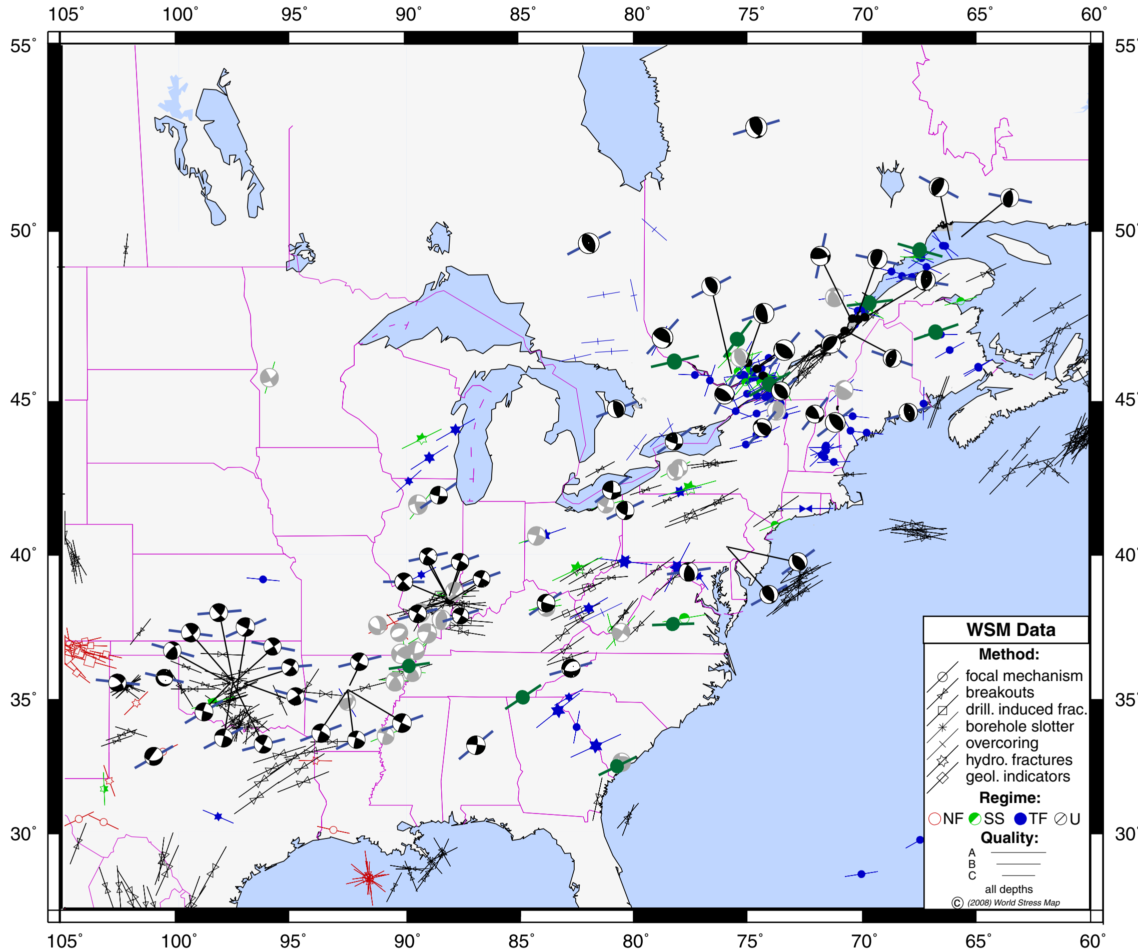

Fig. 1. Stress indicators in the CEUS and SE Canada. Map includes the 52 newly-compiled focal mechanisms (black and white mechanisms with blue bars), 10 stress inversions (dark green circles with dark green bars) and 23 focal mechanisms from Zoback (1992a) (gray mechanisms) overlain on the 2008 World Stress Map. Bars on focal mechanisms and stress inversions represent the approximate and estimated orientation of S_{Hmax}, respectively.

principal stress magnitudes are calculated, changing the overburden gradient does not affect the calculations. The remaining principal stresses are then solved for using two physical constraints. First, the relationship

$$\Phi = \frac{S_2 - S_3}{S_1 - S_3} \quad (1)$$

(after Angelier, 1979), where S_1, S_2 and S_3 represent the three principal stresses in order of decreasing magnitude, places constraints on the potential orientation of slip vectors on the nodal planes. If slip on a nodal plane is geometrically compatible with the local stress field, Φ must fall between 0 and 1 for a given faulting regime. Following the technique of Gephart (1985), Φ is calculated from the orientations of the two focal mechanism nodal planes and the three principal stresses using the following relationship

$$1 - \Phi = -\frac{\beta_{13}\beta_{23}}{\beta_{12}\beta_{22}} = -\frac{\beta_{33}\beta_{23}}{\beta_{32}\beta_{22}} \quad (2)$$

where β_{ij} corresponds to a matrix of angle cosines relating the principal stress and focal mechanism coordinate systems.

A second physical constraint on relative stress magnitudes after Jaeger and Cook (1979) is

$$\frac{S_1 - P_P}{S_3 - P_P} = \left[\left(\mu^2 + 1\right)^{1/2} + \mu\right]^2 \quad (3)$$

where P_P is the pore pressure and μ is the coefficient of fault friction. For given values of P_P and μ, the differential stress magnitudes cannot exceed the stress required to cause shear failure on pre-existing, optimally-oriented faults in the brittle crust. This constraint will be utilized in the next section to evaluate the consistency of shear slip on each of the focal mechanism nodal planes with frictional faulting theory for reasonable values of P_P and μ.

Since Φ provides a measure of the magnitude of S_2 relative to the maximum (S_1) and minimum (S_3) principal stresses, it can be used to map relative stress magnitudes, and therefore faulting styles, across the study area. Following Simpson (1997), we use the Φ values and faulting regimes of each focal mechanism to calculate the AΦ parameter, which scales relative stress magnitudes from 0 to 3 based on faulting style. The relationship is given by:

$$A\Phi = (n + 0.5) + (-1)^n(\Phi - 0.5) \quad (4)$$

Where Φ is calculated in (2) and n = 0, 1 and 2 for normal, strike–slip and reverse faulting types, respectively.

A total of 85 AΦ data points were determined; 52 from focal mechanisms in this study, 10 from stress inversions in this study and 23 from focal mechanisms in Zoback (1992a). The results are shown spatially in Fig. 2. Physically, an AΦ value of 0 represents uniform horizontal extension ($S_V \gg S_{Hmax} = S_{hmin}$), 1.5 represents strike–slip faulting ($S_{Hmax} > S_V > S_{hmin}$) and 3 indicates uniform horizontal compression ($S_{Hmax} = S_{hmin} \gg S_V$). The results illustrate that the horizontal principal stresses become increasingly compressive with

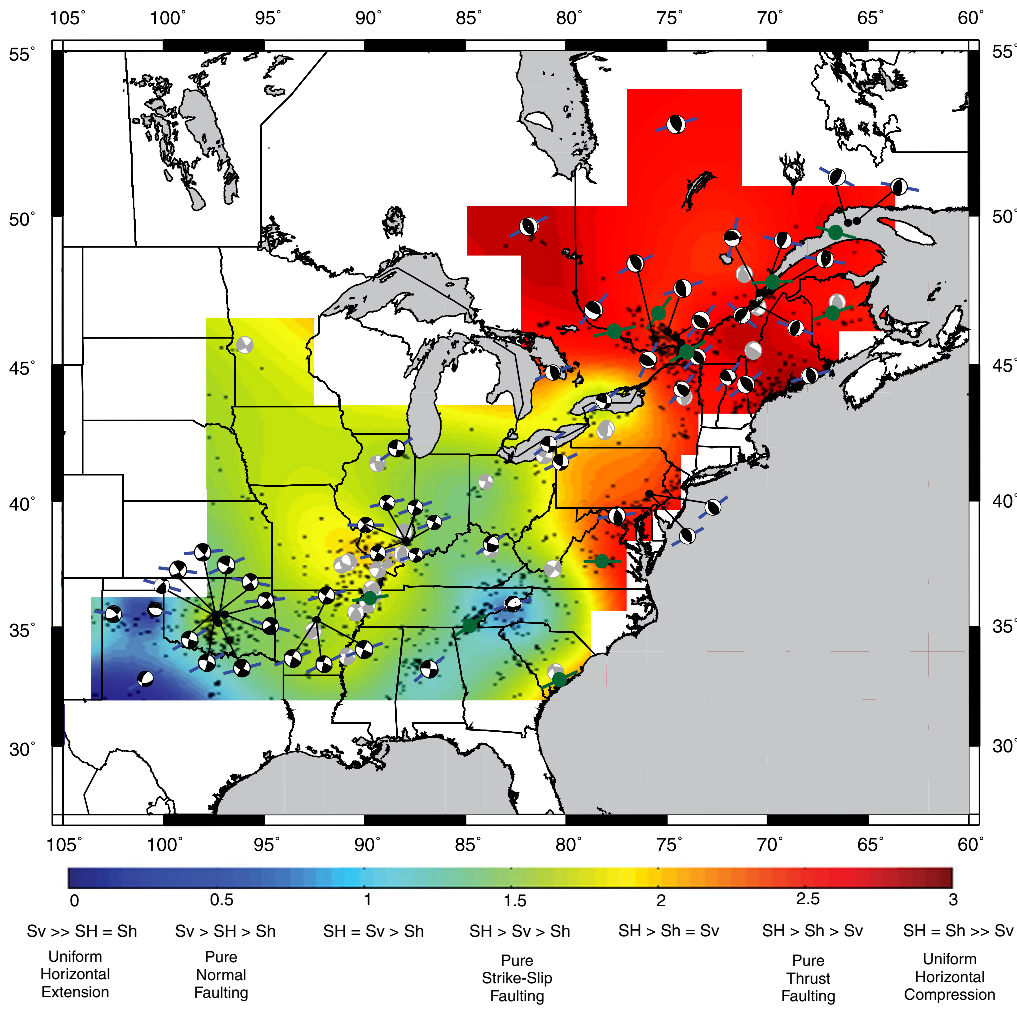

Fig. 2. Spatial variation of the AΦ parameter across the study area. Horizontal stresses become increasingly compressive (AΦ becomes larger in value) with respect to the vertical stress moving from the south-central U.S. to the northeastern U.S. and southeastern Canada. Values are interpolated using a bilinear interpolation scheme, and extrapolated linearly to the boundaries of the map. Background seismicity is from the USGS/NEIC catalog 1973–2010.

respect to the vertical stress moving from the south-central U.S. to the northeastern U.S. and southeastern Canada.

4. Slip compatibility in regional stress field

Our final objective in analyzing the newly-compiled data set is to assess the proximity of each nodal plane in orientation to that expected for shear failure in the local stress field in the context of Mohr–Coulomb failure criterion. We assume P_P is hydrostatic in the brittle crust (following Zoback and Townend, 2001) and μ is consistent with laboratory values determined by Byerlee (1978), who demonstrated that a wide variety of rock types exhibit a coefficient of friction between 0.6 and 1.0 over a wide range of confining pressures. However, to include the possibility that some intraplate faults might have unusually low frictional strength, we evaluate the consistency of slip with the theoretically-predicted planes with values of μ as low as 0.2. Thus, for a given stress orientation and value of Φ, μ and P_P, we determine which of the two nodal planes is more optimally-oriented for shear failure. In other words, our goal is to determine which focal mechanism nodal plane in each pair is closest to the theoretically-expected orientation for failure assuming hydrostatic P_P and μ consistent with laboratory-derived friction values from Byerlee (1978).

A grid search method is utilized to find the most optimally-oriented planes in the local stress field. For each focal mechanism nodal plane pair, the strike on both planes is simultaneously varied from the observed strike by up to ±45°. The nodal plane dips are also varied from the observed dip by up to ±45° while applying the constraint that the dip must be in the range 0–90°. At each strike and dip iteration, the value of μ to fit the observed slip is calculated assuming hydrostatic P_P. Fig. 3 illustrates an example μ map for one of the analyzed earthquakes. The black dots represent the orientations of the preferred (left) and auxiliary (right) nodal planes which were identified based on which plane best fits the assumption of Mohr–Coulomb failure for values of friction between 0.6 and 0.8. Test plane configurations where slip is frictionally impossible in the current stress field are indicated by hatched areas. In the example shown in Fig. 3, the preferred nodal plane is essentially perfectly oriented for a coefficient of friction of about 0.6–0.7. The auxiliary plane would have to be rotated by about 15–20° in strike to be consistent with laboratory-derived friction values.

Fig. 4A displays histograms of the difference in strike and dip between the preferred nodal plane orientation and nearest theoretically-expected nodal plane orientation for μ = 0.6 for all 75 earthquake focal mechanisms considered in this study. The results indicate that overall the orientation of the preferred nodal planes is

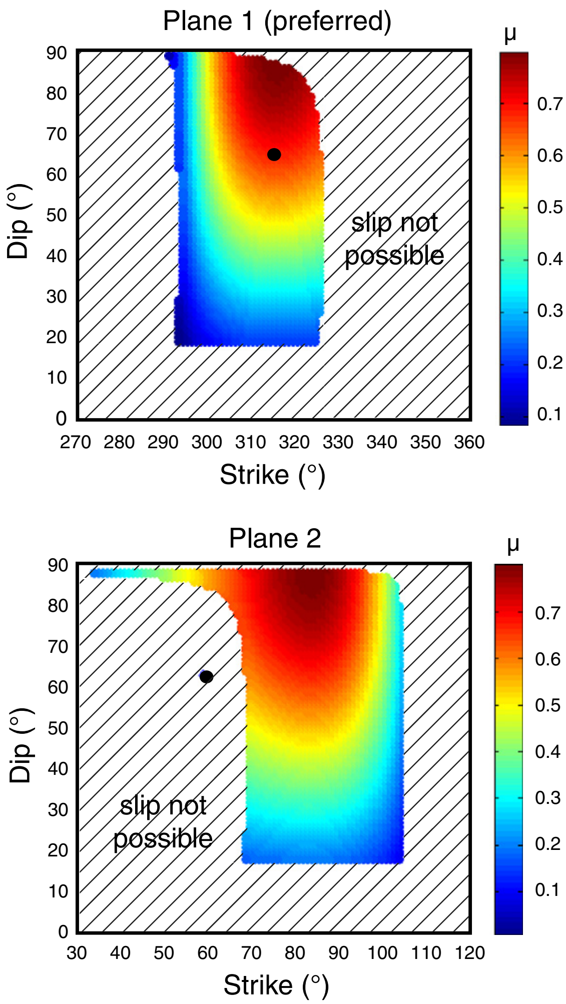

Fig. 3. Example fault friction (μ) map for a single focal mechanism. Black dots represent the orientations of the two nodal planes. Color indicates the μ value required to cause shear failure on a plane with the corresponding strike and dip in the local stress field. Test plane configurations where slip is frictionally impossible in the current stress field are indicated by hatched areas. Plane 1 is the preferred nodal plane as it is closer to the theoretically-expected orientation for μ = 0.6. Event location: NW Texas; Date: 2/10/2010; Location: 35.49° N, 102.65° W; Depth: 13 km; Regime: strike–slip; S_{Hmax}: N 109° E.

quite consistent with the expected orientation for μ = 0.6. The mean mis-fit is only ~7° in strike and dip, which is well within the range of uncertainty associated with the stress orientations and nodal plane determinations. Fig. 4B shows the orientation difference for the conjugate nodal plane for all events, which fit much more poorly. Finally, Fig. 5 shows the mis-fit of the preferred plane in strike and dip with a theoretically-ideal plane for assumed friction values of 0.2, 0.6 and 0.8. Note that a coefficient of friction of 0.6 is much more consistent with the observations than either the higher or lower friction values.

5. Discussion

5.1. The stress field in the central and eastern US

In agreement with previous observations, the newly compiled focal mechanisms and stress inversions suggest a highly consistent NE–SW S_{Hmax} orientation throughout the CEUS and southeastern Canada (Fig. 1). Such large-scale uniform stress fields are typically thought to be the result of buoyancy-driven forces such as ridge push and internal density heterogeneities in the lithosphere (Zoback and Zoback, 2007) or from geoid perturbations and mantle thermal anomalies (Davies, 1999). The central Virginia, Charlevoix, St. Lawrence and New Madrid seismic zones all contain evidence for local rotations of S_{Hmax} from this general trend. Note that the stress rotations within these seismic zones are frequently supported by numerous individual focal mechanism stress indicators occurring on different faults over a variety of depths.

Many of these second-order stress orientations have been observed for several decades, and the physical processes generating such seismicity may include buoyancy-driven forces from deglaciation or sediment loading and lower crustal heterogeneities. Baird et al. (2010), in using 3D numerical modeling techniques to predict spatial locations of seismicity in the Charlevoix seismic zone, illustrated the importance of a detailed structural understanding of ancient fault zones and how slip on pre-existing structures may potentially modify the local stresses, and therefore the seismicity distribution and faulting type (see also Mazzotti and Townend, 2010).

5.2. Relative stress magnitudes and faulting styles

The AΦ parameter is used to map relative stress magnitudes and faulting styles across the study area. Our results indicate a clear contrast between primarily thrust faulting mechanisms in southeastern Canada and the northeastern United States and dominantly strike–slip faulting mechanisms moving toward the south-central United States (Figs. 1 and 2). In other words, the horizontal stresses become increasingly compressive with respect to the vertical stress moving from the south-central to the northeast U.S. and southeastern Canada. One mechanism discussed for producing these relative principal stress contrasts has been the superposition of stresses in relation to unloading of a massive Pleistocene ice sheet (e.g. Clark, 1982; James, 1991; James and Bent, 1994; Stein et al., 1979; Wu and Hasegawa, 1996; Wu and Johnston, 2000; Wu and Mazzotti, 2007). These models typically assumed a disk-shaped load applied on a layered earth model with either elastic or viscous lithosphere properties and generally matched the contrast in relative stress magnitudes in a qualitative sense. However, as Zoback (1992a) noted, glacial rebound models are often inconsistent with the observed sense of relative stress contrasts between southeastern Canada and the eastern United States and produce stress perturbations that are too small to account for the observed stress change at seismogenic depths when superimposed on the ambient stress field. Zoback and Mooney (2003) discussed the possibility that relatively high compression in the northeastern U.S. and southeastern Canada might be related to negative buoyancy effects associated with relatively high density in the mantle lithosphere which “pulls down” on the crust and increases compression.

Baird et al. (2010) noted that active faulting in southeastern Canada may be related to the orientation of paleotectonic rift structures with respect to the modern day regional stress field. For example, many seismic zones in southeastern Canada fall along pre-existing NW-SE trending structures, such as the Ottawa and Saguenay grabens, which are perpendicular to the orientation of S_{Hmax} and thus more likely for reactivation through thrust faulting. Conversely, strike–slip faulting in the CEUS may result from a general NE–SW trend of ancient rift structures combined with a slightly rotated ENE–WSW S_{Hmax} orientation, which makes the structures more favorable for reactivation in a strike–slip sense.

The analysis used to examine relative stress magnitudes and faulting styles in this study could be extended to other continental regions where a relatively small set (20–40) of well-constrained and well-distributed focal mechanisms is available. Western Europe,

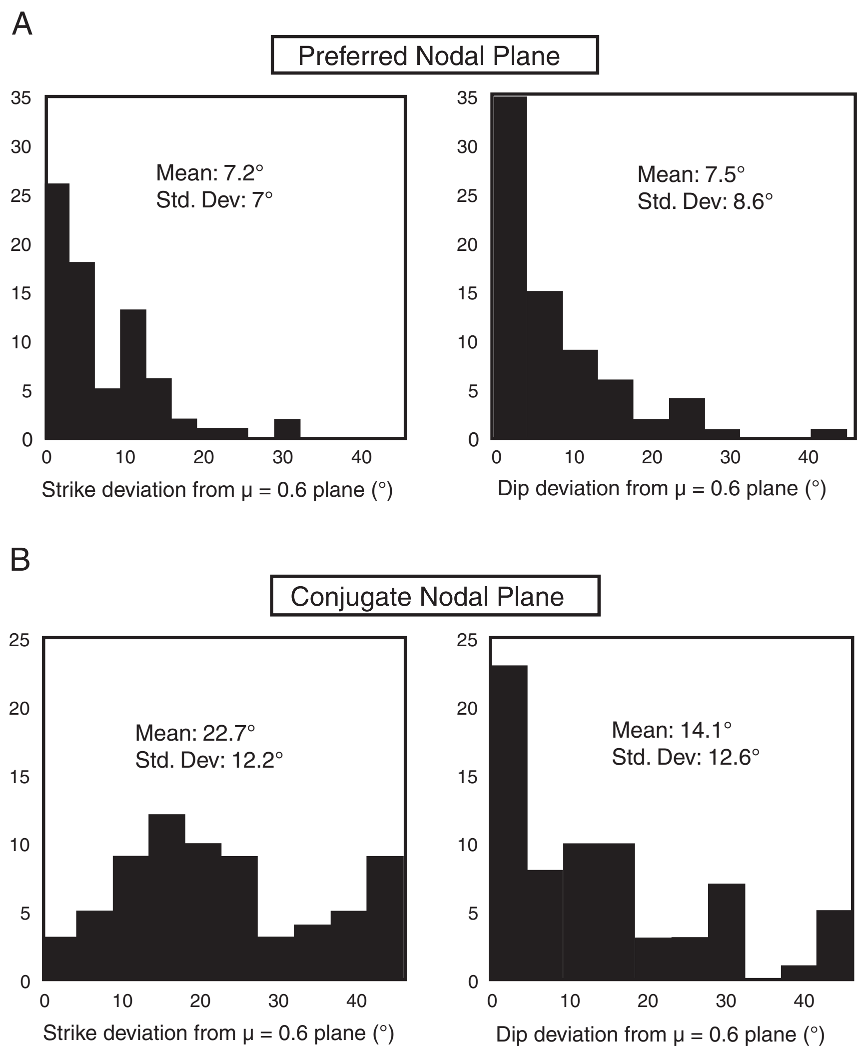

Fig. 4. Histograms showing the mis-fit in strike and dip between (A) the preferred and (B) the conjugate nodal planes and the theoretically optimally-oriented ($\mu = 0.6$) fault plane for all 75 focal plane mechanisms. Most preferred nodal planes strike and dip within 8° of the theoretically optimally-oriented fault plane. Note the different frequency scales between the preferred and conjugate nodal plane histograms.

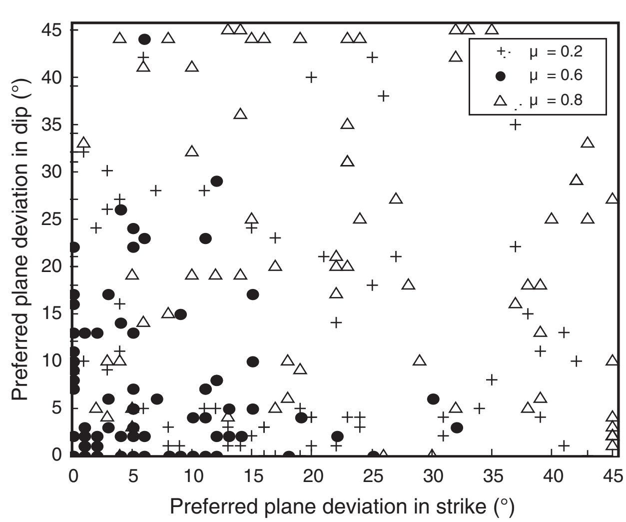

Fig. 5. Mis-fit in strike and dip between the preferred nodal planes and the nearest nodal planes that fail with $\mu = 0.2$, $\mu = 0.6$ and $\mu = 0.8$. A coefficient of friction of 0.6 is much more consistent with the observations than higher or lower friction values.

China, Central Asia and NW South America all represent regions of extensive seismic activity, and would perhaps be the most feasible candidates for a similar study. The AΦ parameter in particular may help illuminate spatial transitions between a range of faulting types in structurally and tectonically complex regions.

5.3. Slip compatibility and fault friction

For each nodal plane pair for all 75 earthquakes, we select one nodal plane as being preferentially-oriented for shear failure in the local stress field on the basis of its proximity to the nearest plane compatible with Mohr–Coulomb failure with $\mu = 0.6$. The vast majority of these preferred nodal planes are within 7° in strike and dip from a fault plane that fails with $\mu = 0.6$ (Fig. 4a), and we interpret these planes to be generally compatible with shear failure in the local stress field. We interpret the results in terms of a rotated nodal plane pair about a stationary stress tensor, although since we assume the three principal stresses lie in vertical and horizontal planes the analysis is equivalent to rotating a stress tensor about fixed nodal planes. Regardless of reference frame, only small perturbations are required for the preferred nodal planes to be optimally-oriented for shear failure in the local stress field.

We consider coefficients of friction (μ) between 0.6 and 0.8 for our analysis based on several lines of evidence. First, Byerlee (1978) demonstrated from laboratory experiments on a wide variety of rock types over a range of confining pressures that μ generally takes a value between 0.6 and 1.0, although it may be lower in shaly rocks, which is not relevant to the earthquakes studied here. Second, in-situ stress measurements extending to as deep as ~9 km in the upper crust are regularly consistent with predicted stress magnitudes using Coloumb frictional-failure theory with $0.6 \leq \mu \leq 1.0$ (e.g. Fig. 1 in Townend and Zoback, 2000). Thirdly, Sibson and Xie (1998) and Collettini and Sibson (2001) demonstrated using the Coulomb failure criterion that the dip range of active thrust and normal faults is consistent with fault reactivation assuming $0.6 \leq \mu \leq 0.85$ and principal stresses lying in horizontal and vertical planes. While their studies considered only fault planes which produced moderate to large earthquakes ($M > 5.5$), which is notably larger than the majority of earthquakes examined in this study, their results support our prescribing laboratory-consistent friction coefficients to seismogenic faults in the crust.

Gudmundsson et al. (2010) demonstrated that variable physical properties within major fault zones, specifically within the damage zone and fault core, can affect local stress orientations and magnitudes, which may subsequently influence fracture propagation behavior. Our analysis directly examines whether or not local stress perturbations, anomalous fault friction, or elevated pore pressures are required to explain the observed slip on intraplate faults in a relatively uniform regional stress field. Specifically, we consider the slip compatibility of focal mechanism nodal planes with friction coefficients as low as 0.2 and as high as 0.8. The results demonstrate that slip on the vast majority of nodal planes is consistent with laboratory-derived friction coefficients assuming hydrostatic pore pressure in the brittle crust.

Our assumption of hydrostatic pore pressure is based on widespread observations of hydrostatic pore pressure persisting to as deep as 12 km in the upper crust (Table 1 in Townend and Zoback, 2000) and the consistency of hydrostatic pore pressure in the upper crust with maintaining observed lithospheric deformation rates in force-limited stress models (Zoback and Townend, 2001). While we acknowledge that faults can be conduits for fluid flow and elevated pore pressures, our results suggest that, in terms of the regional stress field, there is generally no reason to call on elevated P_P to explain the occurrence of intraplate earthquakes. Our slip compatibility results are consistent with the analysis of Zoback (1992a), and are in agreement with the hypothesis that the brittle crust is generally in a state of frictional failure equilibrium due to regional plate driving forces (Zoback et al., 2002) and local perturbations associated with variations of lithospheric density (Zoback and Mooney, 2003).

6. Conclusions

(1) Newly compiled stress data including 75 earthquake focal plane mechanisms and 10 formal stress inversions from the central and eastern United States and southeastern Canada indicate a highly consistent, compressional, NE–SW oriented maximum horizontal stress across much of intraplate North America. The new data are consistent with many pre-existing stress measurements from a wide variety of stress indictors.

(2) Using the AΦ parameter calculated from the orientation of the focal mechanism nodal planes and the stress tensor at each earthquake location, we investigate the variation in relative stress magnitudes and faulting type across the study area. There is a clear transition from predominantly strike–slip faulting in the south-central U.S. to predominantly thrust faulting in the NE U.S. and southeastern Canada which reflects increasingly compressive (higher AΦ values) horizontal stresses with respect to the vertical stress moving from central to NE North America.

(3) Using Mohr–Coulomb failure criterion and assuming hydrostatic pore pressure, we find the vast majority of preferred focal mechanism nodal planes are consistent in orientation with optimally-oriented planes ($\mu = 0.6$) for shear failure in the local stress field. This suggests that shear failure on the preferred nodal planes generally do not require reduced fault friction or elevated pore pressures.

Acknowledgements

Support during this research for O. Hurd came from Achievement Rewards for College Scientists (ARCS) fellowships and from the Stanford University Geophysics Department. We thank Agust Gudmudsson, John Townend and I. Balintoni for their critical reviews and constructive comments that improved the manuscript.

Appendix A

New focal plane mechanisms compiled for this study. Tectonic regime assigned based on criteria from M.L. Zoback (1992b); N = normal, SS = strike–slip, and T = thrust. Preferred nodal plane is indicated in bold. Δstr and Δdip are mis-fits between the preferred nodal plane and the theoretically optimally-oriented nodal plane ($\mu = 0.6$). P and T-axes plunges are measured from horizontal. *m_N.

Date yyyy/mm/dd	Lat (°N)	Long (°W)	Z (km)	M_W	Strike (°)	Dip (°)	Rake (°)	P-axis (Az°:Pl°)	T-axis (Az°:Pl°)	Type	Location	S_H Azi (N °E)	Φ	Δstr (°)	Δdip (°)	Ref
1988/09/07	38.14	83.88	10	4.6	**198**	**51**	**−178**	55:28	160:25	SS	NW Kentucky	72	0.683	18	2	3
					107	88	−39									
1993/11/16	45.20	73.46	12	3.9	**144**	**45**	**96**	50:0	142:86	T	Napierville, Canada	41	0.697	28	1	2
					316	45	84									
1994/01/16	40.34	76.01	2	3.9	156	45	108	53:1	150:77	T	Reading, PA	63	0.432	6	1	2
					311	**48**	**73**									
1994/01/16	40.31	76.04	3	4.6	**135**	**49**	**68**	241:2	336:73	T	Wyomissing Hills, PA	63	0.131	9	1	1
					347	46	144									
1995/06/16	44.29	71.91	6	3.7	**95**	**50**	**40**	38:6	300:53	T	Lisbon, NH	52	0.143	10	5	2
					337	61	132									
1996/03/14	45.99	74.43	18	3.7	**136**	**36**	**98**	40:9	191:80	T	Lachute, Canada	41	0.233	6	11	2
					306	54	84									
1996/08/21	44.18	71.35	7	3.4	**144**	**60**	**93**	232:15	62:75	T	Berlin, NH	41	0.885	0	13	2
					318	30	85									
1997/05/24	45.81	74.19	22	3.6	**96**	**33**	**60**	27:15	256:68	T	Christieville, Canada	41	0.212	4	17	2
					311	62	108									

Appendix A (*continued*)

Date yyyy/mm/dd	Lat (°N)	Long (°W)	Z (km)	M_W	Strike (°)	Dip (°)	Rake (°)	P-axis (Az°:Pl°)	T-axis (Az°:Pl°)	Type	Location	S_H Azi (N °E)	Φ	Δstr (°)	Δdip (°)	Ref
1997/10/28	47.67	69.91	5	4.3	**27**	**66**	**111**	102:20	334:59	T	Charlevoix, Canada	49	0.678	5	22	2
					164	31	51									
1997/11/06	46.75	71.35	22	4.5	39	63	87	131:18	302:72	T	Quebec City, Canada	63	0.736	3	10	2
					226	**27**	**96**									
1998/07/30	46.17	72.74	12	3.7	150	27	75	71:19	272:70	T	La Conception, Canada	50	0.859	15	18	2
					347	**64**	**98**									
1998/09/25	41.50	80.39	2	4.5	**9**	**69**	**144**	64:8	327:40	T	Pymatuning, PA	71	0.054	5	14	2
					114	57	25									
1999/03/16	49.65	66.39	18	4.4	**30**	**63**	**93**	118:18	307:72	T	Gaspe Penin., Canada	60	0.945	0	17	2
					203	27	84									
2000/01/01	46.87	78.90	13	5.1	**116**	**68**	**69**	222:20	354:61	T	Temiskaming, Canada	60	0.714	4	22	2
					342	30	132									
2000/04/20	43.95	74.25	8	3.6	150	54	120	219:5	119:66	T	Saranac Lake, NY	67	0.396	0	1	2
					286	**46**	**55**									
2001/01/26	41.99	80.83	2	3.9	**5**	**79**	**159**	53:7	320:23	SS	Ashtabula, OH	69	0.001	4	26	2
					99	69	12									
2002/06/05	52.85	74.35	2	3.6	**145**	**55**	**65**	253:7	0:69	T	Quebec, Canada	105	0.59	2	10	6
					4	42	121									
2002/06/18	37.99	87.77	18	4.6	**297**	**84**	**−8**	252:10	343:01	SS	Caborn, IN	93	0.669	11	8	4
					28	82	−174									
2003/06/13	47.70	70.09	9	3.3	**80**	**70**	**60**	192:19	312:55	T	Quebec, Canada	37	0.671	1	25	6
					319	36	144									
2004/08/04	43.67	78.23	4	3.1	106	77	32	234:12	331:31	SS	Port Hope, Lake Ontario	79	0.731	23	2	5
					8	**59**	**165**									
2005/08/25	35.88	82.80	8	3.7	**90**	**60**	**−60**	49:62	159:10	N	Western North Carolina	62	0.597	3	7	6
					221	41	−131									
2005/10/20	44.68	80.48	10	3.6	167	67	101	249:22	97:66	T	Quebec, Canada	79	0.201	1	11	6
					320	**25**	**65**									
2006/04/07	47.38	70.46	25	3.8	15	55	85	109:10	266:79	T	Quebec, Canada	65	0.809	3	10	6
					204	**35**	**97**									
2006/10/03	44.33	68.17	2	3.9	**166**	**55**	**93**	254:10	90:79	T	Bar Harbor, ME	20	0.929	0	3	6
					340	35	85									
2006/12/07	49.51	81.54	16	4.2*	148	46	84	242:1	343:86	T	Kapuskasing, Canada	41	0.804	13	2	7
					337	**44**	**96**									
2008/04/18	38.45	87.89	14	5.2	25	90	−175	250:4	160:4	SS	SE Illinois	92	0.165	10	9	6
					295	**85**	**0**									
2008/04/18	38.48	87.89	14	4.6	135	90	−10	90:7	180:7	SS	SE Illinois	92	0.517	1	3	6
					225	**80**	**−180**									
2008/04/21	38.47	87.82	15	4.0	**210**	**85**	**175**	255:0	165:7	SS	SE Illinois	92	0.341	10	23	6
					300	85	5									
2008/04/25	38.45	87.87	13	3.7	**204**	**85**	**170**	250:4	159:11	SS	SE Illinois	92	0.116	9	41	6
					295	80	5									
2008/06/05	38.45	87.87	17	3.4	305	90	20	78:14	172:14	SS	SE Illinois	92	0.687	11	6	6
					215	**70**	**180**									
2008/10/14	35.76	100.70	11	3.7	**276**	**64**	**−106**	157:67	18:18	N	NW Texas	136	0.237	5	5	6
					130	30	−60									
2008/11/15	47.74	69.72	14	3.6	175	55	70	279:8	34:72	T	Quebec, Canada	53	0.465	6	2	6
					27	**40**	**116**									
2009/04/21	33.01	87.14	5	3.8	**275**	**85**	**−10**	230:11	321:3	SS	Central Alabama	70	0.957	12	9	6
					6	80	−175									
2009/07/21	49.81	65.71	15	3.5	360	60	75	101:14	236:71	T	Quebec, Canada	60	0.479	6	2	6
					208	**33**	**114**									
2010/01/15	35.59	97.26	8	3.8	**145**	**90**	**25**	277:17	13:17	SS	Central Oklahoma	69	0.059	4	44	6
					55	65	180									
2010/01/15	35.57	97.28	8	3.7	**135**	**85**	**30**	265:17	3:24	SS	Central Oklahoma	69	0.124	8	43	6
					42	60	174									
2010/01/24	35.57	97.28	6	3.6	115	85	25	246:14	342:21	SS	Central Oklahoma	69	0.406	0	1	6
					23	**65**	**174**									
2010/02/04	35.49	102.65	13	3.3	**315**	**65**	**−30**	276:38	7:1	SS	NW Texas	109	0.734	6	8	6
					59	63	−152									
2010/02/10	41.97	88.49	11	3.8	9	85	170	55:4	324:11	SS	NE Illinois	48	0.372	5	0	6
					100	**80**	**5**									
2010/02/13	35.53	97.30	5	3.2	**57**	**80**	**−170**	281:14	191:0	SS	Central Oklahoma	69	0.254	1	4	6
					325	80	−10									
2010/02/27	35.54	96.75	4	4.2	**40**	**80**	**−160**	265:21	172:7	SS	Central Oklahoma	69	0.957	0	24	6
					306	70	−11									
2010/03/22	35.54	96.74	8	3.7	**57**	**86**	**−150**	285:24	187:17	SS	Central Oklahoma	69	0.978	0	10	6
					325	60	−5									
2010/06/23	45.86	75.46	22	5.0	145	60	80	242:14	30:73	T	Southern Quebec	41	0.531	3	16	6
					344	**31**	**107**									
2010/07/16	39.17	77.25	18	3.4	**195**	**57**	**123**	262:7	159:62	T	Western Maryland	38	0.466	9	15	6
					325	45	50									
2010/08/08	32.99	100.79	4	3.4	**203**	**61**	**−132**	60:53	322:6	N	West Central Texas	80	0.578	19	5	6
					85	50	−40									

(*continued on next page*)

Appendix A (*continued*)

Date yyyy/mm/dd	Lat (°N)	Long (°W)	Z (km)	M_W	Strike (°)	Dip (°)	Rake (°)	P-axis (Az°:Pl°)	T-axis (Az°:Pl°)	Type	Location	S_H Azi (N °E)	Φ	Δstr (°)	Δdip (°)	Ref
2010/09/16	35.63	97.22	4	3.3	285	85	10	59:3	150:11	SS	Central Oklahoma	69	0.43	8	0	6
					194	**80**	**175**									
2010/09/19	35.60	97.21	3	3.4	195	90	160	242:14	148:14	SS	Central Oklahoma	69	0.346	10	6	6
					285	**70**	**0**									
2010/10/11	35.31	92.32	5	4.0	**202**	**80**	**165**	249:4	158:18	SS	Central Arkansas	84	0.219	5	25	6
					295	75	10									
2010/10/11	35.31	92.33	4	3.6	**197**	**80**	**165**	244:4	153:18	SS	Central Arkansas	84	0.377	11	23	6
					290	75	10									
2010/10/13	35.20	97.31	14	4.3	29	85	170	75:4	344:11	SS	Central Oklahoma	69	0.353	4	0	6
					120	**80**	**5**									
2010/10/14	35.3	92.35	4	3.4	115	90	−5	70:4	160:4	SS	Central Arkansas	84	0.780	13	6	6
					205	**85**	**−180**									
2010/10/15	35.28	92.32	5	3.8	211	85	−170	76:11	345:4	SS	Central Arkansas	84	0.531	13	1	6
					120	**80**	**−5**									

References
1) Ammon, C.J., Herrmann, R.B., Langston, C.A., Benz, H.M., 1998. Faulting parameters of the January 16, 1994 Wyomissing Hills, Pennsylvania earthquakes. Seis. Res. Lett. 69, 261–269.
2) Du, W.-X., Kim, W.-Y., Sykes, L.R., 2003. Earthquake source parameters and state of stress for the northeastern United States and southeastern Canada from analysis of regional seismograms. Bull. Seis. Soc. Am. 93, 1633–1648.
3) Street, R., Taylor, K., Jones, D., Harris, J., Steiner, G., Zekulin, A., Zhang, D., 1993. The 4.6 mbLg northeastern Kentucky earthquake of September 7, 1988. Seis. Res. Lett. 64, 187–199.
4) Kim, W.-Y., 2003. The 18 June 2002, Caborn, Indiana, earthquake: Reactivation of ancient rift in the Wabash Valley seismic zone? Bull. Seis. Soc. Am. 93, 2201–2211.
5) Kim, W.-Y., Dineva, S., Ma, S., Eaton, D., 2006. The 4 August 2004, Lake Ontario, earthquake. Seis. Res. Lett. 77, 65–73.
6) St. Louis University Earthquake Center, 2010. http://www.eas.slu.edu/Earthquake_Center/MECH.NA/index.html. Last accessed September 2010.
7) Ma, S., Eaton, D.W., Adams, J., 2008. Intraplate seismicity of a recently deglaciated shield terrane: A case study from northern Ontario, Canada. Bull. Seis. Soc. Am. 98, 2828–2848.

Appendix B

New formal stress inversions compiled for study. SS = strike–slip, T = thrust. All data are from Mazzotti and Townend (2010).

Lat (°N)	Long (°W)	σ_1 Az (°)	Type	N	Φ	Seismic zone
49.35	66.59	104	T	12	0.6	Lower St. Lawrence (Canada)
47.9	69.67	86	T	60	0.7	Charlevoix (Canada)
48.68	75.23	38	T	19	0.2	Gatineau (Canada)
46.03	77.40	78	T	8	0.7	Ottawa (Canada)
45.13	74.09	58	T	21	0.6	Montreal (Canada)
46.76	66.55	70	T	12	0.4	North Appalachian (Canada)
37.78	78.23	90	T	13	0.3	Central Virginia
35.27	84.60	54	SS	26	0.8	East Tennessee
36.12	89.67	82	SS	18	0.1	New Madrid (Missouri)
32.92	80.47	64	SS	11	0	Charleston (South Carolina)

Appendix C

Focal mechanisms from M.L. Zoback (1992a). N = normal, SS = strike–slip, TS = transpressive and T = thrust. Preferred nodal plane is indicated in bold. Δstr and Δdip are mis-fits between the preferred nodal plane and the theoretically optimally-oriented nodal plane (μ = 0.6). P and T-axes plunges are measured from horizontal. See Zoback (1992a) for citations.

Date yyyy/mm/dd	Lat (°N)	Long (°W)	Z (km)	Mw	Strike (°)	Dip (°)	Rake (°)	P-axis (Az°:Pl°)	T-axis (Az°:Pl°)	Type	Location	S_H Azi (N °E)	Φ	Δstr (°)	Δdip (°)
1988/11/25	48.12	71.18	29.0	5.9	**207**	**41**	**144**	81/15	192/54	T	Saguenay, Canada	60	0.31	8	0
					326	67	55								
1979/08/19	47.67	69.90	10.0	5	152	43	22	106/20	356/44	TS	Charlevoix, Canada	60	0.54	25	0
					46	**76**	**131**								
1982/01/09	47.00	66.60	7.0	5.7	332	49	59	264/01	172/67	T	Miramachi, Canada	65	0.54	1	1
					195	**50**	**121**								
1978/02/18	46.3	74.1	7	4.1	**345**	**39**	**97**	250/04	40/81	T	St. Donat, Canada	55	0.61	0	8
					156	51	84								
1975/07/09	45.7	96	7.5	4.6	**60**	**70**	**0**	17:14	283:14	SS	Western Minnesota	50	0.26	8	14
					150	90	−160								

Appendix C (*continued*)

Date yyyy/mm/dd	Lat (°N)	Long (°W)	Z (km)	Mw	Strike (°)	Dip (°)	Rake (°)	P-axis (Az°:Pl°)	T-axis (Az°:Pl°)	Type	Location	S_H Azi (N °E)	Φ	Δstr (°)	Δdip (°)
1973/06/15	45.3	70.9	6	5	**185**	**23**	**153**	47:32	187:15	SS	Quebec-Maine	60	0.73	16	9
					300	80	70								
1983/10/07	43.94	74.26	7.5	5.1	342	31	106	277:15	68:73	T	Goodnow, New York	70	0.51	1	13
					180	**60**	**81**								
1967/06/13	42.9	78.2	3	4.4	130	47	37	74:11	336:53	T	Attica, New York	70	0.26	5	13
					13	**64**	**131**								
1966/01/01	42.8	78.2	2	4.8	110	70	20	62:01	331:28	SS	Attica, New York	70	0.18	1	13
					13	**71**	**159**								
1986/01/31	41.65	81.16	7	5	**115**	**71**	**10**	75:07	342:21	SS	Perry, Ohio	70	0.24	2	2
					22	81	161								
1972/09/15	41.6	89.4	13	4.4	**170**	**70**	**160**	38:1	129:28	SS	Platform, Illinois	55	0.34	12	8
					267	71	21								
1986/07/12	40.55	84.39	5	4.5	**288**	**80**	**10**	244:14	334:0	SS	St. Mary, Ohio	75	0.72	11	7
					20	80	−170								
1987/06/10	38.71	87.95	10	4.9	**136**	**70**	**15**	89:4	357:24	SS	Olney, Illinois	75	0.2	11	4
					41	76	160								
1974/04/03	38.6	88.1	15	4.7	**310**	**70**	**0**	267:14	173:14	SS	Illinois Basin	75	0.54	9	6
					220	90	160								
1980/07/27	38.17	83.91	18	5.2	**30**	**60**	**180**	251:21	349:21	SS	Sharpsburg, Kentucky	65	0.35	5	5
					300	90	−30								
1968/11/09	38	88.5	22	5.5	**195**	**45**	**101**	97:1	192:82	T	Illinois Basin	75	0.67	6	1
					359	46	79								
1965/08/14	37.2	89.3	1.5	3.8	**280**	**70**	**−20**	239:28	148:1	SS	Illinois Basin	80	0.32	6	0
					17	71	−159								
1962/02/02	36.5	89.6	7.5	4.3	84	55	7	43:19	301:28	SS	NW rift, Missouri	75	0.35	6	44
					350	**84**	**145**								
1975/06/13	36.5	89.7	9	4.2	**85**	**60**	**−20**	49:34	313:8	SS	NW rift, Missouri	75	0.09	6	2
					186	73	−149								
1970/11/17	35.9	89.9	16	4.4	**319**	**61**	**18**	272:9	176:32	SS	Rift axis, Arkansas	75	0.38	14	2
					220	75	150								
1976/03/25	35.6	90.5	12	5	**323**	**63**	**28**	272:1	181:38	SS	Rift axis, Arkansas	75	0.20	13	5
					220	65	150								
1967/06/04	33.6	90.9	12	4.5	**292**	**70**	**10**	248:7	155:21	SS	Western Mississippi	70	0.21	5	2
					200	80	160								
1972/02/03	33.31	80.58	2	4.5	**259**	**40**	**9**	221:28	107:38	SS	Bowman, South Carolina	55	0.1	3	3
					162	84	130								

References

Angelier, J., 1979. Determination of the mean principal directions of stresses for a given fault population. Tectonophysics 56, T17–T26.

Baird, A.F., McKinnon, S.D., Godin, L., 2010. Relationship between structures, stress and seismicity in the Charlevoix seismic zone revealed by 3-D geomechanical models: implications for the seismotectonics of continental interiors. Journal of Geophysical Research 115, B11402.

Bott, M.H.P., 1959. The mechanics of oblique slip faulting. Geological Magazine 96, 109–117.

Byerlee, J.D., 1978. Friction of rock. Pure and Applied Geophysics 116, 615–626.

Clark, J.A., 1982. Glacial loading: A cause of natural fracturing and a control of the present stress state in regions of high Devonian shale gas. paper SPE 10798 presented at Unconventional Gas Recovery Symposium, Soc. Pet. Eng., Pittsburgh, Pa., May 16–18.

Collettini, C., Sibson, R.H., 2001. Normal faults, normal friction? Geology 29, 927–930.

Davies, G.F., 1999. Dynamic earth plates, plumes and mantle convection. Cambridge University Press, Cambridge, UK. 458 pp.

Gephart, J.W., 1985. Principal stress directions and the ambiguity in fault plane identification from focal mechanisms. Bulletin of the Seismological Society of America 75, 621–625.

Gephart, J.W., Forsyth, D.D., 1984. An improved method for determining the regional stress tensor using earthquake focal mechanism data: application to the San Fernando earthquake sequence. Journal of Geophysical Research 89, 9305–9320.

Gudmundsson, A., Simmenes, T.H., Larsen, B., Philipp, S.L., 2010. Effects of internal structure and local stresses on fracture propagation, deflection, and arrest in fault zones. Journal of Structural Geology 32, 1643–1655.

Heidbach, O., Tingay, M., Barth, A., Reinecker, J., Kurfeß, D., Müller, B., 2008. The world stress map database release 2008. (http://www.world-stress-map.org. August 2010).

Jaeger, J.C., Cook, N.G.W., 1979. Fundamentals of Rock Mechanics. Chapman and Hall, London, UK. 475 pp.

James, T.S., 1991. Post-glacial deformation. Ph.D. thesis. Princeton University Press, Princeton, N.J. 190 pp.

James, T.S., Bent, A.L., 1994. A comparison of eastern North American seismic strain-rates to glacial rebound strain-rates. Geophysical Research Letters 21, 2127–2130.

Khattri, K., 1973. Earthquake focal mechanism studies – a review. Earth-Science Reviews 9, 19–63.

Kisslinger, C., Bowman, J.R., Koch, K., 1981. Procedures for computing focal mechanisms from local (SV/P) data. Bulletin of the Seismological Society of America 71, 1179–1729.

Lay, T., Wallace, T.C., 1995. Modern Global Seismology. Academic Press, San Diego. 521 pp.

Mazzotti, S., Townend, J., 2010. State of stress in central and eastern North American seismic zones. Lithosphere 2, 76–83.

McKenzie, D.P., 1969. The relation between fault plane solutions for earthquakes and the directions of the principal stresses. Bulletin of the Seismological Society of America 59, 591–601.

Michael, A.J., 1984. Determination of stress from slip data: faults and folds. Journal of Geophysical Research 89, 11517–11526.

Nábělek, J.L., 1984. Determination of earthquake source parameters from inversion of body waves. Ph.D. Thesis, Massachusetts Institute of Technology, Cambridge, MA.

Sbar, M.L., Sykes, L.R., 1973. Contemporary compressive stress and seismicity in eastern North America: an example of intra-plate tectonics. Geological Society of America Bulletin 84, 1861–1882.

Sibson, R.H., Xie, G., 1998. Dip range for intracontinental reverse fault ruptures: truth not stranger than friction ? Bulletin of the Seismological Society of America 88, 1014–1022.

Simpson, R.W., 1997. Quantifying Anderson's fault types. Journal of Geophysical Research 102, 17909–17919.

Stein, S., Sleep, N.H., Geller, R.J., Wang, S.-C., Kroeger, G.C., 1979. Earthquakes along the passive margin of eastern Canada. Geophysical Research Letters 6, 537–540.

Sykes, L.R., 1978. Intraplate seismicity, reactivation of preexisting zones of weakness, alkaline magmatism, and other tectonism postdating continental fragmentation. Reviews of Geophysics and Space Physics 16, 621–688.

Townend, J., Zoback, M.D., 2000. How faulting keeps the crust strong. Geology 28, 399–402.

Wu, P., Hasegawa, H.S., 1996. Induced stresses and fault potential in eastern Canada due to a disc load: a preliminary analysis. Geophysical Journal International 125, 415–430.

Wu, P., Johnston, P., 2000. Can deglaciation trigger earthquakes in N. America? Geophysical Research Letters 27, 1323–1326.

Wu, P., Mazzotti, S., 2007. Effects of a lithospheric weak zone on postglacial seismotectonics in eastern Canada and northeastern USA. In: Stein, S., Mazzotti,

S. (Eds.), Continental intraplate earthquakes: Science, hazard and policy issues: Geo. Soc. Am. Special Paper, 425, pp. 113–128.
Zoback, M.L., 1992a. Stress field constraints on intraplate seismicity in eastern North America. Journal of Geophysical Research 97, 11761–11782.
Zoback, M.L., 1992b. First- and second-order patterns of stress in the lithosphere: the World Stress Map Project. Journal of Geophysical Research 97, 11703–11728.
Zoback, M.L., Mooney, W.D., 2003. Lithospheric buoyancy and continental intraplate stress. International Geology Review 45, 95–118.
Zoback, M.D., Townend, J., 2001. Implications of hydrostatic pore pressures and high crustal strength for the deformation of intraplate lithosphere. Tectonophysics 336, 19–30.
Zoback, M.D., Townend, J., Grollimund, B., 2002. Steady-state failure equilibrium and deformation of intraplate lithosphere. International Geology Review 44, 383–401.
Zoback, M.D., Zoback, M.L., 1981. State of stress and intraplate earthquakes in the United States. Science 213, 96–104.
Zoback, M.D., Zoback, M.L., 1991. Tectonic stress field of North America and relative plate motion. In: Slemmon, B., et al. (Ed.), The geology of North America, Decade Map Volume 1, Neotectonics of North America. Geol. Soc. Am., Boulder, Colorado, pp. 339–366.
Zoback, M.L., Zoback, M.D., 1980. State of stress of the conterminous United States. Journal of Geophysical Research 85, 6113–6156.
Zoback, M.L., Zoback, M.D., 2007. Lithosphere Stress and Deformation. In: Watts, A., Schubert, G. (Eds.), Earthquake Seismology. : Treatise on Geophysics, vol. 6. Elsevier Ltd., Amsterdam, pp. 253–274.